

**Description of hot and dense hadron-gas properties in a new excluded-volume model**

S. K. Tiwari,\* P. K. Srivastava, and C. P. Singh

*Department of Physics, Banaras Hindu University, Varanasi 221005, India*

(Received 10 November 2011; published 17 January 2012)

A new equation of state for a hot and dense hadron gas (HG) is obtained where the finite hard-core size of baryons has been incorporated into a thermodynamically consistent formulation of excluded volume correction. Our model differs from other existing approaches on the following points. We assign a hard-core volume only to each baryon and mesons, which, although they possess a small volume, can fuse and interpenetrate into one another. Use of the full quantum statistics is made to obtain the grand canonical partition function, where excluded-volume correction has been incorporated by explicitly integrating over volume. We thus find that the new model works even for cases of extreme temperatures and/or densities where most other approaches fail. The numerical calculation indicates that the causality is respected by our prescription even at extreme densities. The temperature and density dependences of various thermodynamical quantities, e.g., pressure, baryon density, entropy and energy density, compare well with the results of other microscopic HG models. After suitable parametrization of the center-of-mass energy in terms of temperature and baryon chemical potential, we explore some new freeze-out criteria which exhibit full independence of the collision energy and of the structures of the colliding nuclei. We further demonstrate the suitability of our model for explaining the various experimental results of the multiplicity ratios of various particles and their antiparticles. Finally, we use our excluded-volume model to obtain the transport behavior of a hot and/or dense HG, such as shear viscosity- to-entropy ratio and speed of sound, and compare the results with earlier calculations.

DOI: [10.1103/PhysRevC.85.014908](https://doi.org/10.1103/PhysRevC.85.014908)

PACS number(s): 24.10.Pa, 12.38.Mh, 12.38.Gc, 25.75.Nq

**I. INTRODUCTION**

One of the most important predictions of quantum chromodynamics (QCD) regards the phase transition from a hot, dense hadron gas (HG) to a deconfined and/or chiral symmetric plasma of quarks and gluons called quark-gluon plasma (QGP) that occurs at a high temperature and/or baryon density. However, despite extensive experimental and/or theoretical research work performed during the last three decades, precise qualitative and quantitative predictions for many aspects of this phase transition are still missing [1–6]. Even the phase diagram for the phase transition is quite uncertain and still exists as a conjectured one. Ultrarelativistic heavy-ion collisions offer the best method for studying the properties of QGP in the laboratory. However, direct observation of primordial plasma is impossible in the laboratory due to the confinement problem. Moreover, QGP survives for a very brief time only, and hence after subsequent expansion and cooling, QGP finally hadronizes into a dense and hot HG [7]. Thus QGP diagnostics becomes a very complicated field of study because of our limited knowledge of the HG background. In this context, the search for a proper equation of state (EOS) is of extreme importance because it can suitably describe the properties of hot and dense HG. There are compelling reasons for investigating the properties of HG in unusual environments, in particular, at high temperatures and/or baryon densities. The cosmological situations after the big bang, the interior of neutron stars, and the matter produced in the laboratory after ultrarelativistic heavy-ion collisions are all governed by the presence of such HG matter, and hence a proper EOS

can help us to analyze the properties of the matter in above systems. In an IHG description, all mesons and baryons are treated as pointlike and noninteracting. However, using Gibb's construction of equilibrium phase transition between HG and QGP, we find an anomalous phase reversal from QGP to HG at large  $\mu_B$  and  $T$  in the IHG picture [8]. This anomalous situation is usually cured by assigning a finite and hard-core volume to each baryon, which results in a strong repulsive force between a pair of baryons or antibaryons. Thus any fireball created in a heavy-ion collision at a fixed  $T$  and  $\mu_B$  cannot accommodate more than a limiting number of baryons because its volume becomes completely occupied. Moreover, it restricts the mobility of the baryons in the fireball, and as a consequence, the thermodynamic pressure of HG is also considerably reduced. Does this kind of "jamming" also result in a phase transition as we often notice, e.g., in the percolation theory? Therefore, it is worthwhile to study in detail a statistical thermodynamic model in which the geometrical hard-core volume of each baryon has been incorporated as an excluded-volume effect [8]. The purpose of this paper is, first, to formulate a new thermodynamically consistent excluded-volume model where we assign a finite hard-core volume to each baryon, but mesons in the theory can easily overlap, fuse, and interpenetrate into each other. Second, an excluded-volume correction is obtained by performing an explicit integration over the "available" volume in the grand canonical partition function. Third, we use full quantum statistics so that our formulation is valid for extreme cases of temperature/density. Our model differs from others mainly regarding the above features. Here we wish to examine the predictions of our model and make a detailed comparison with the experimental results. We emphasize that we have used this model successfully to obtain the conjectured QCD phase boundary and thus determine precisely the location of

\* sktiwari4bhu@gmail.com

the QCD critical end point [9,10]. We have also calculated the freeze-out curve and we note that the critical end point indeed exists almost on the freeze-out curve. The plan of this paper runs as follows: the ensuing section is devoted to the model description and we derive our version of the thermodynamically consistent EOS for a hot, dense HG. Then we calculate different thermodynamical quantities such as the number density, energy density, entropy density, and pressure of HG and compare our model calculations with other calculations [11]. In the next section, we analyze the experimental data on particle multiplicities and ratios for central nucleus-nucleus collision in terms of our model over a broad energy range, from the lowest GSI Schwerionen Synchrotron (SIS) energy to the highest Relativistic Heavy Ion Collider (RHIC) energies, to extract the chemical freeze-out temperatures and baryon chemical potentials, which are then suitably parametrized in terms of the center-of-mass energies, and subsequently some chemical freeze-out criteria are also deduced. Thermal fits computed within the statistical models have often been used to successfully reproduce the hadron yield ratios obtained in experimental heavy-ion collisions [12–20]. We use our freeze-out picture for calculating the hadron multiplicities and ratios of strange and nonstrange hadrons and compare our results with the experimental data. We also predict the hadron yields which we expect at the Large Hadron Collider (LHC) energy. We further use this prescription to calculate pion and nucleon densities, and a good comparison between our calculation and Hanbury-Brown-Twiss (HBT) experimental data demonstrates the validity of our model. We also investigate the validity of different freeze-out criteria in our model and conclude that at chemical freeze-out, the energy per particle in the fireball  $E/N \approx 1$  and the entropy per particle  $S/N \approx 7.0$  emerge as the most appropriate criteria, which are almost independent of the collision energies and structures of colliding nuclei. In order to make the discussion complete, we further derive  $\eta/s$  and the speed of sound from our model and compare them with other models. In the concluding section, we focus our attention on the hadron ratios where our model fails and that warrant an exotic phenomenon, e.g., QGP formation, as a suitable alternative to understand them properly.

## II. MODEL DESCRIPTION

We briefly describe our derivation of the EOS for the HG, based on the excluded-volume correction [8,21], where we have assigned a hard-core size to all baryons, while mesons are still treated as pointlike particles in the grand canonical partition function. Moreover, unlike in our previous paper [8], where Boltzmann statistics make the calculation simple, here we use the full quantum statistics. Thus the grand canonical partition function can be written as follows:

$$\ln Z_i^{\text{ex}} = \frac{g_i}{6\pi^2 T} \int_{V^0}^{V - \sum_j N_j V_j^0} dV \times \int_0^\infty \frac{k^4 dk}{\sqrt{k^2 + m_i^2}} \frac{1}{\left[ \exp\left(\frac{E_i - \mu_i}{T}\right) + 1 \right]}, \quad (1)$$

where  $g_i$  is the degeneracy factor of the  $i$ th species of baryons,  $E_i$  is the energy of the particle ( $E_i = \sqrt{k^2 + m_i^2}$ ),  $V_i^0$  is the eigenvolume assigned with each baryon of the  $i$ th species, and hence  $\sum_j N_j V_j^0$  becomes the total occupied volume, where  $N_j$  represent the total number of baryons of the  $j$ th species. We can clearly write Eq. (1) as

$$\ln Z_i^{\text{ex}} = V \left( 1 - \sum_j n_j^{\text{ex}} V_j^0 \right) I_i \lambda_i, \quad (2)$$

where  $I_i$  represents the integral

$$I_i = \frac{g_i}{6\pi^2 T} \int_0^\infty \frac{k^4 dk}{\sqrt{k^2 + m_i^2}} \frac{1}{\left[ \exp\left(\frac{E_i}{T}\right) + \lambda_i \right]}, \quad (3)$$

and  $\lambda_i = \exp\left(\frac{\mu_i}{T}\right)$  is the fugacity of the particle;  $n_i^{\text{ex}}$  is the number density after excluded-volume correction and can be obtained from Eq. (2) as

$$n_i^{\text{ex}} = \frac{\lambda_i}{V} \left( \frac{\partial \ln Z_i^{\text{ex}}}{\partial \lambda_i} \right)_{T,V}. \quad (4)$$

Thus our prescription is thermodynamically consistent and it leads to a transcendental equation,

$$n_i^{\text{ex}} = (1 - R) I_i \lambda_i - I_i \lambda_i^2 \frac{\partial R}{\partial \lambda_i} + \lambda_i^2 (1 - R) I_i', \quad (5)$$

where  $I_i'$  is the partial derivative of  $I_i$  with respect to  $\lambda_i$ , and  $R = \sum_i n_i^{\text{ex}} V_i^0$  is the fractional occupied volume. We can write  $R$  in an operator equation form as [9]:

$$R = R_1 + \hat{\Omega} R, \quad (6)$$

where  $R_1 = \frac{R^0}{1 + R^0}$ , and  $R^0 = \sum_i n_i^0 V_i^0 + \sum_i I_i' V_i^0 \lambda_i^2$ ;  $n_i^0$  is the density of pointlike baryons of the  $i$ th species, and the operator  $\hat{\Omega}$  has the form

$$\hat{\Omega} = -\frac{1}{1 + R^0} \sum_i n_i^0 V_i^0 \lambda_i \frac{\partial}{\partial \lambda_i}. \quad (7)$$

Using the Neumann iteration method and retaining the series up to the  $\hat{\Omega}^2$  term, we get

$$R = R_1 + \hat{\Omega} R_1 + \hat{\Omega}^2 R_1. \quad (8)$$

After solving Eq. (8), we finally get the expression of total pressure [21] for the HG as

$$P^{\text{ex}} = T(1 - R) \sum_i I_i \lambda_i + \sum_i P_i^{\text{meson}}. \quad (9)$$

Here  $P_i^{\text{meson}}$  is the pressure due to the  $i$ th type of meson.

In Eq. (9), the first term represents the pressure due to all types of baryons, where excluded-volume correction is incorporated, and the second term gives the pressure arising due to all mesons in HG as if they possess a pointlike size. This makes it clear that we consider the repulsion arising only between a pair of baryons and/or antibaryons because we assign them exclusively a hard-core volume. In order to make the calculation simple, we have taken an equal volume  $V^0 = 4\pi r^3/3$  for each type of baryon with a hard-core radius  $r = 0.8$  fm. We have considered in our calculations all baryons and mesons and their resonances having masses up to a cutoff value of 2 GeV/ $c^2$  and lying in the HG spectrum. Here

only resonances having well-defined masses and widths have been incorporated in the calculations. Branching ratios for sequential decays have been suitably accounted for, and in the presence of several decay channels, only the dominant mode is included. We have also strictly imposed the condition of strangeness neutrality by putting  $\sum_i S_i (n_i^s - \bar{n}_i^s) = 0$ , where  $S_i$  is the strangeness quantum number of the  $i$ th hadron, and  $n_i^s (\bar{n}_i^s)$  is the strange (antistrange) hadron density, respectively. Using this constraint equation, we get the value of the strange chemical potential in terms of  $\mu_B$ . Having done all these things, we proceed to calculate the energy density of each baryon species  $i$  using the following formula:

$$\epsilon_i^{\text{ex}} = \frac{T^2}{V} \frac{\partial \ln Z_i^{\text{ex}}}{\partial T} + \mu_i n_i^{\text{ex}}. \quad (10)$$

Similarly, the entropy density is

$$s = \frac{\epsilon_i^{\text{ex}} + P^{\text{ex}} - \mu_B n_B - \mu_S n_S}{T}. \quad (11)$$

It is evident that this approach is more simple in comparison to other thermodynamically consistent, excluded-volume approaches, which often possess transcendental final expressions that are usually found to be difficult to solve [14]. This approach does not involve any arbitrary parameter in the calculation. Moreover, this approach can be used for extremely low as well as extremely high values of  $T$  and  $\mu_B$  where all other approaches fail to give a satisfying result [14].

### III. HADRONIC PROPERTIES

In this section, we attempt to calculate the number density, pressure, energy density, and entropy density of hadrons and compare the results with the predictions of a microscopic model named the URASiMA generator [11], which is essentially based on the molecular-dynamical simulation performed for a system of hadrons. In Fig. 1, we show the variation of the total number density of hadrons with respect to the temperature at a fixed baryon density and compare it with the results obtained by the URASiMA event generator. The results show a very close agreement between our model calculation and the results of Sasaki, but at higher  $T$ , the curves seem to differ slightly.

In Fig. 2, we have plotted the variation of the total pressure generated by all hadrons with respect to temperature at a fixed net baryon density. The hadronic pressure initially shows a very slow increase, but for  $T \geq 170$  MeV, the pressure increases rapidly. The hadronic pressure calculated in our model again shows a good agreement with the results of Sasaki [11]. This shows that the EOS of HG as given by our excluded-volume model incorporating macroscopic geometrical features gives results in close agreement with the simulation involving hadrons and hadronic interactions. The method of Sasaki [11] involves various parameters, e.g., coupling constants of hadron, arising due to hadronic interactions. However, it is encouraging to see such excellent matching of the results obtained with two very different models.

Figure 3 represents the variation of the energy density of HG with respect to temperature at a constant net baryon density. Again, the very good agreement between our model

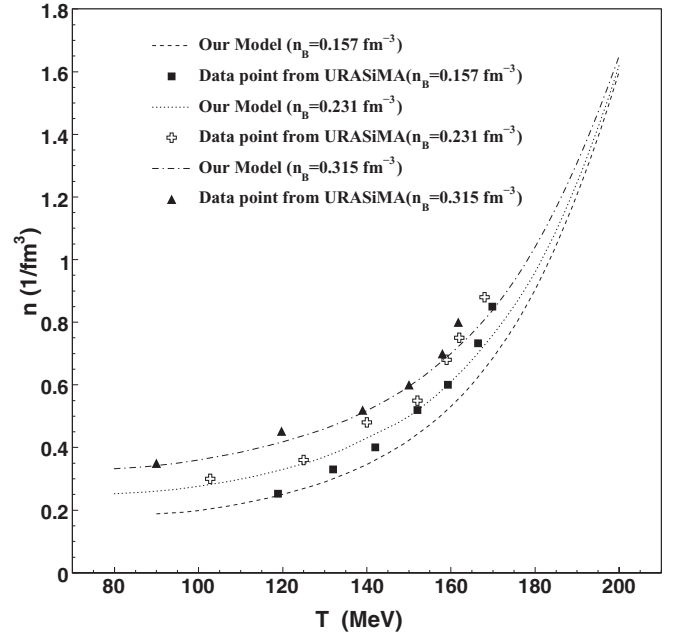


FIG. 1. Variation of total number density with respect to temperature at a constant net baryon density. Lines show our model calculation while symbols are the data calculated by Sasaki using the URASiMA event generator.

calculations and the results from the URASiMA event generator demonstrates the validity of our model in describing the properties of hot, dense HG. The energy density increases very slowly with the temperature initially and then increases rapidly at higher temperatures. Similarly, in Fig. 4, we show the variation of entropy per baryon  $s/n_B$  in an HG with respect

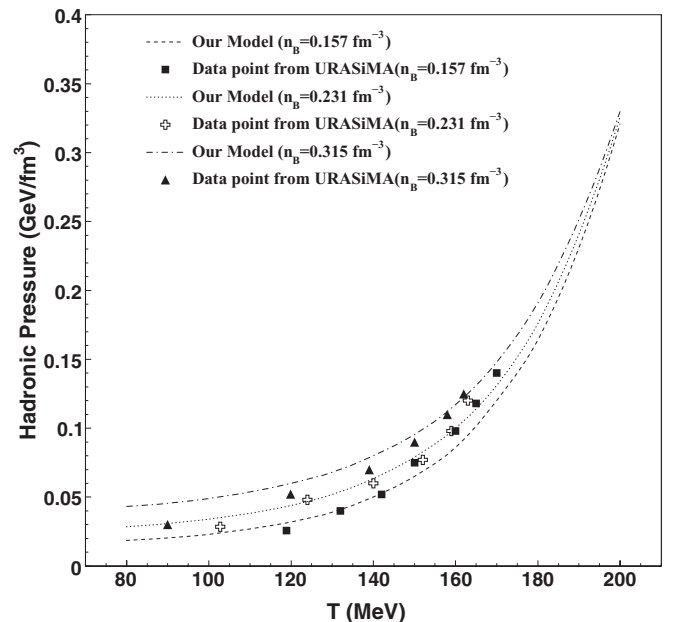


FIG. 2. Variation of pressure with respect to temperature at a constant net baryon density. Lines show our model calculation while symbols are the data calculated by Sasaki using the URASiMA event generator.

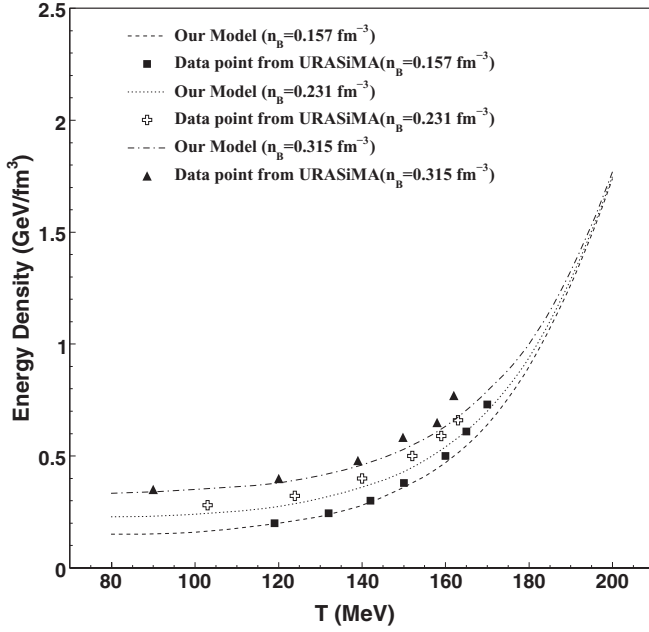


FIG. 3. Variation of energy density with respect to temperature at a constant net baryon density. Lines show our model calculation while symbols are the data calculated by Sasaki using the URASiMA event generator.

to the temperature at a fixed net baryon density. We stress that  $s/n_B$  measures the yield of all particles relative to nucleons [22], and the IHG model gives  $s/n_B$  as an almost-constant quantity for any fireball, which means that it does not change during the expansion or evolution of the fireball. So this is a measurable quantity and is significant in fixing the properties of the HG. Again, Fig. 4 demonstrates a very good agreement between the two models. It should be stressed here that the essential difference between the present model and the earlier calculation [8] is the use of full quantum statistics here, in comparison to the Boltzmann statistics used in Ref. [8]. We note that this modification has improved the fit between our model and Sasaki's calculation. Both models predict a rapid increase in  $s/n_B$  for  $T \geq 160$  MeV even at a fixed  $n_B$ .

In order to relate the thermal parameters of hot, dense HG with the center-of-mass energy, we extract them by fitting the experimental particle ratios from the lowest SIS energy

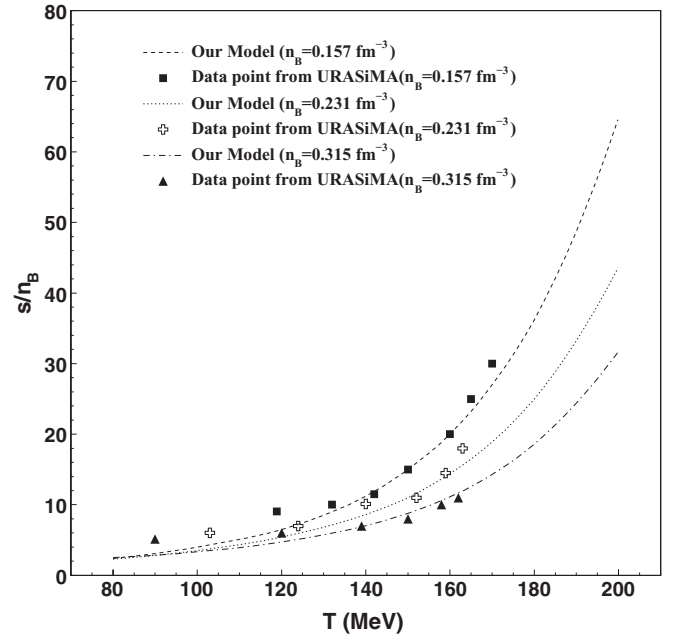


FIG. 4. Variation of  $s/n_B$  with respect to temperature at a constant net baryon density. Lines show our model calculation while symbols are the data calculated by Sasaki using the URASiMA event generator.

to the highest RHIC energy by our model calculation. We thus deduce the temperature and baryon chemical potential thermodynamically from the experiments at various energies as listed in Table I. For comparison, we have also shown the values obtained in other models, e.g., the ideal hadron gas (IHG) and Rischke, Gorenstein, Stöcker, and Greiner (RGSG) models. We then parametrize the variables  $T$  and  $\mu_B$  in terms of center-of-mass energy as follows [23]:

$$\mu_B = \frac{a}{1 + b\sqrt{s_{NN}}}, \quad (12)$$

$$T = c - d\mu_B^2 - e\mu_B^4. \quad (13)$$

where the parameters  $a$ ,  $b$ ,  $c$ ,  $d$ , and  $e$  have been determined from the best fit:  $a = 1.482 \pm 0.0037$  GeV,  $b = 0.3517 \pm 0.009$  GeV<sup>-1</sup>,  $c = 0.163 \pm 0.0021$  GeV,  $d = 0.170 \pm 0.02$  GeV<sup>-1</sup>, and  $e = 0.015 \pm 0.01$  GeV<sup>-3</sup>.

TABLE I. Thermal parameter ( $T$ ,  $\mu_B$ ) values obtained by fitting the experimental particle ratios in different model calculations.

| $\sqrt{s_{NN}}$ (GeV) | IHG model |         |            | RGSG model |         |            | Our old model |         |            | Our present model |         |            |
|-----------------------|-----------|---------|------------|------------|---------|------------|---------------|---------|------------|-------------------|---------|------------|
|                       | $T$       | $\mu_B$ | $\delta^2$ | $T$        | $\mu_B$ | $\delta^2$ | $T$           | $\mu_B$ | $\delta^2$ | $T$               | $\mu_B$ | $\delta^2$ |
| 2.70                  | 60        | 740     | 0.85       | 60         | 740     | 0.75       | 60            | 740     | 0.87       | 70                | 760     | 1.15       |
| 3.32                  | 80        | 670     | 0.89       | 78         | 680     | 0.34       | 90            | 670     | 0.69       | 90                | 670     | 0.45       |
| 3.84                  | 100       | 645     | 0.50       | 86         | 640     | 0.90       | 100           | 650     | 0.60       | 100               | 640     | 0.34       |
| 4.32                  | 101       | 590     | 0.70       | 100        | 590     | 0.98       | 101           | 600     | 0.53       | 105               | 600     | 0.23       |
| 8.76                  | 140       | 380     | 0.45       | 145        | 406     | 0.62       | 140           | 380     | 0.26       | 140               | 360     | 0.25       |
| 12.3                  | 148       | 300     | 0.31       | 150        | 298     | 0.71       | 148.6         | 300     | 0.31       | 150               | 276     | 0.20       |
| 17.3                  | 160       | 255     | 0.25       | 160        | 240     | 0.62       | 160.6         | 250.6   | 0.21       | 155               | 206     | 0.27       |
| 130                   | 172.3     | 35.53   | 0.10       | 165.5      | 38      | 0.54       | 172.3         | 28      | 0.056      | 163.5             | 32      | 0.05       |
| 200                   | 172.3     | 23.53   | 0.065      | 165.5      | 25      | 0.60       | 172.3         | 20      | 0.043      | 164               | 20      | 0.05       |

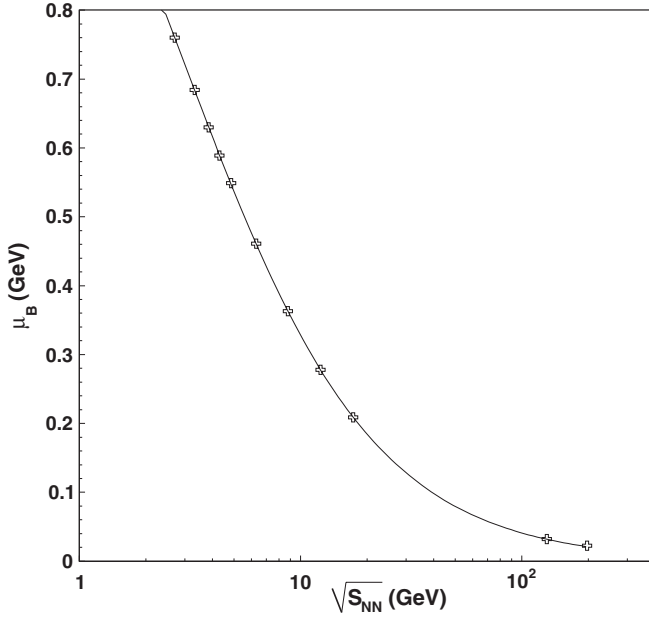


FIG. 5. Variation of chemical potential with respect to center-of-mass energy.

In this exercise we have used full-phase-space  $4\pi$  data, but at RHIC energies midrapidity data are available for all the ratios and hence they are accordingly used, so that we can remove any possible influence on particle ratios arising due to hydrodynamical flow [24]. This allows us to study the hadronic ratios without bothering about the expansion of the system at freeze-out. However, we have used RHIC data available at midrapidity at energies of 130 and 200 GeV, respectively. Moreover, the midrapidity and full-phase-space data at these

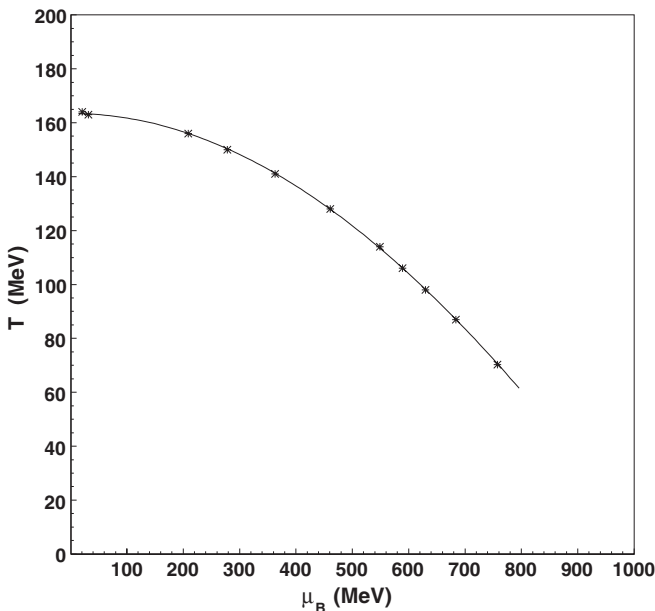


FIG. 6. Variation of chemical freeze-out temperature with respect to baryon chemical potential.

energies differ only slightly as pointed out by Alt *et al.* for  $K^+/\pi^+$  and  $K^-/\pi^-$  ratios [26].

In Fig. 5, we show the parametrization of the freeze-out values of the baryon chemical potential with respect to the center-of-mass energy, and similarly, in Fig. 6, we show the chemical freeze-out curve between temperature and baryon chemical potential. The fits demonstrate that the parameters in parametrizations (12) and (13) have been suitably chosen and the experimental variable such as center-of-mass energy can be described well by the variables  $T$  and  $\mu_B$  of the fireball.

#### IV. ENERGY DEPENDENCE OF HADRON RATIOS

In a series of measurements of Pb-Pb and Au-Au collisions at various center-of-mass energies [30–34], it is found that there is an unusually sharp variation giving rise to peaks in the  $K^+/\pi^+$  and  $\Lambda/\pi^-$  ratios. Such a strong variation of  $K^+/\pi^+$  with energy does not occur in  $p$ - $p$  collisions and, therefore, has been attributed to the presence of unusual phenomena of the QGP formation. This transition is referred as the “horn” in Ref. [30]. A strong variation of  $\Lambda/\pi^-$  with energy has also been attributed as a signal for the existence of a critical point in the QCD phase diagram [35,36] and nontrivial information about the critical temperature  $T_C \approx 176$  MeV has been extracted [36]. A sharp rise at low energies, with a mild maximum and a subsequent flattening of  $K^+/\pi^+$ , was also reported by many authors [15,18,37] using various statistical model calculations. Nayak *et al.* [38] have also explained the horn by using a microscopic approach for the HG. Similarly, a good fit with the experimental data for the horn has been proclaimed as the onset of QGP formation [39–41]. In Fig. 7, we show the results of our calculation for  $K^+/\pi^+$  and we compare our results

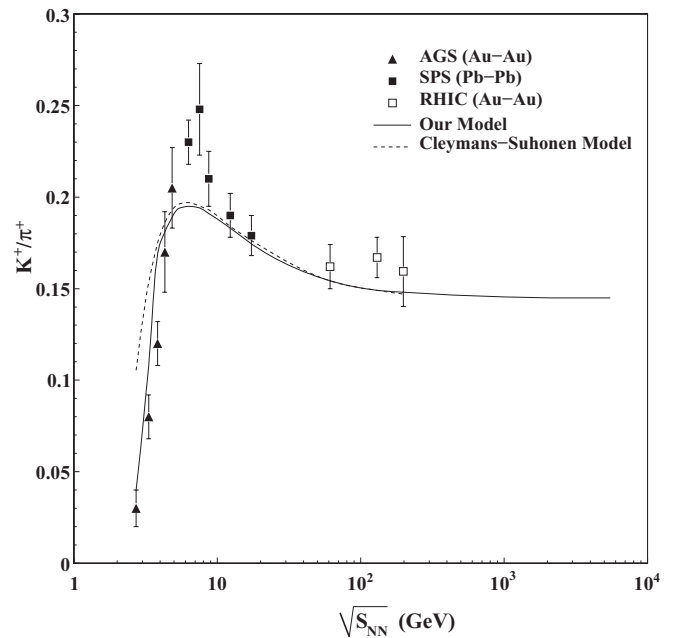


FIG. 7. Energy dependence of  $K^+/\pi^+$  ratio. We compare our results with the Cleymans-Suhonen model [25]. Symbols are experimental data [26–29]. RHIC data are at midrapidity.

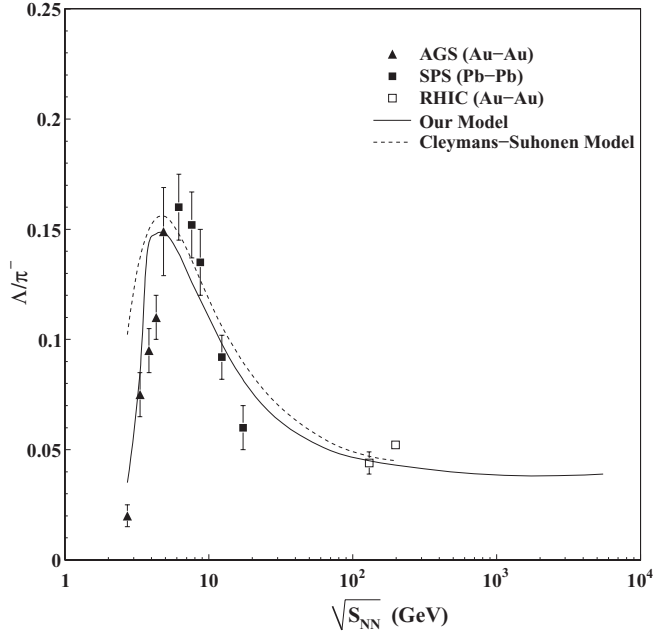


FIG. 8. Energy dependence of  $\Lambda$  relative to pion. We compare our results with the Cleymans-Suhonen model [25]. Symbols are experimental data [26–29]. RHIC data are at midrapidity.

with those from other models. We find that our results almost coincide with the results of the Cleymans-Suhonen model, which involves a thermodynamical inconsistency. Figure 8 shows the variation of  $\Lambda/\pi^-$  with  $\sqrt{s_{NN}}$ . We have again compared our results with various HG models [25] and we find that our model calculation gives a much better fit to the experimental data at all energies in comparison to other models. Although we have not successfully reproduced the sharp peak in  $K^+/\pi^+$ , we still get a broad peak, and our results almost reproduce the data at lower as well as higher energies. In the  $\Lambda/\pi^-$  case we get a sharp peak around the center-of-mass energy of 5 GeV and our results almost reproduce all the features of the experimental data.

In Figs. 9 and 10, we show the variations of the multiplicity ratios of  $\phi$  and  $\Omega$  relative to pions with the center-of-mass energy, respectively. Our model is able to reproduce the experimental data only at lower  $\sqrt{s_{NN}}$ . Although our model calculation is not able to describe these ratios, it is closer to the experimental data in comparison to other models, especially at higher  $\sqrt{s_{NN}}$ . We note that no thermal model can suitably account for the multiplicity ratios of multistrange particles since  $\Omega^-$  is  $sss$  and  $\phi$  is  $s\bar{s}$  hidden-strange quark combinations. Strangeness enhancement invoked in the case of QGP formation will also give nonmatching results. However, the quark coalescence model assuming QGP formation has been claimed to explain the results [42]. In the thermal model, this result for multistrange particles raises doubt about the degree of chemical equilibration for strange hadrons reached in the HG fireball. The failures of excluded-volume models in these cases may indicate the presence of QGP formation. Figure 11 shows the energy dependence of  $K^-$  and  $p$  relative to pions. There is a very good agreement between our model calculations and the experimental data. These ratios saturate at

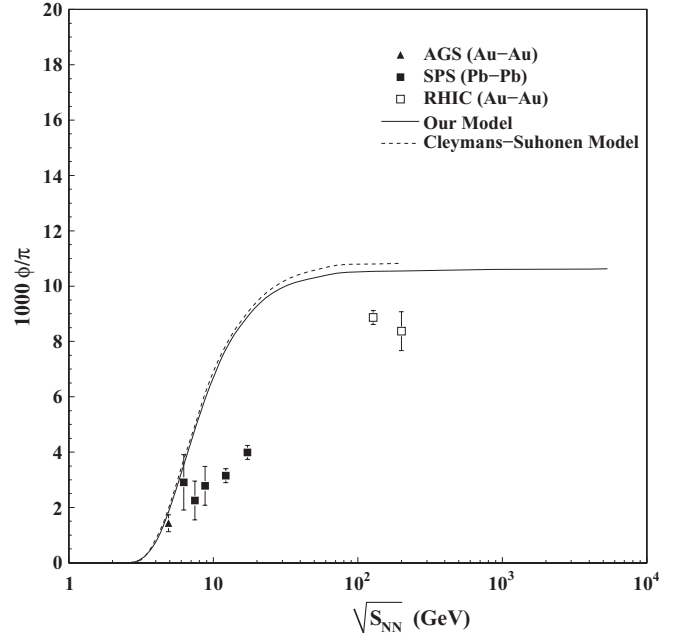


FIG. 9. Energy dependence of  $\phi$  relative to pion. We compare our results with the Cleymans-Suhonen model [25]. Symbols are experimental data [26–29]. RHIC data are at midrapidity.

higher energies, which means that the production rate of these particles is independent of  $\sqrt{s_{NN}}$  at higher energies. In Fig. 12, we show the energy dependence of antiparticle-to-particle ratios, e.g.,  $K^-/K^+$ ,  $\bar{p}/p$ ,  $\bar{\Lambda}/\Lambda$ , and  $\bar{\Xi}^+/\Xi^-$ . These ratios increase sharply with respect to  $\sqrt{s_{NN}}$  and then almost saturate at higher energies, reaching the value 1.0 at the LHC energy. This behavior shows that the production rates of antiparticles relative to particles continuously increase with increasing

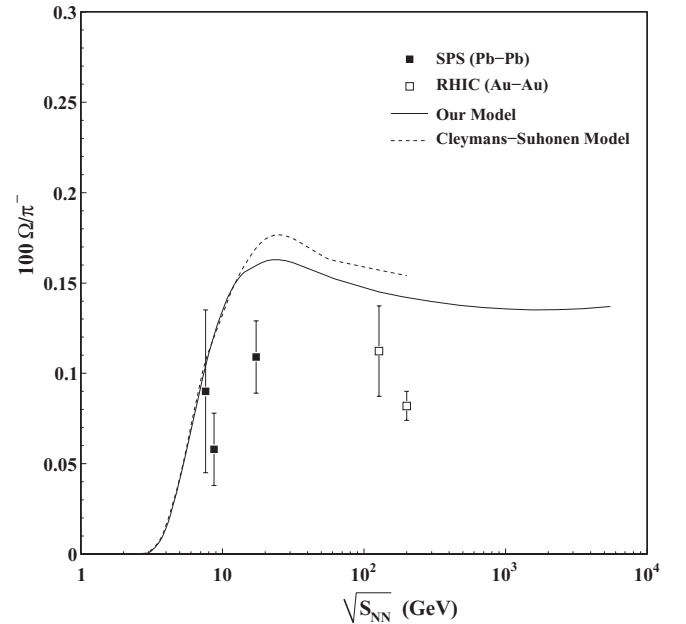


FIG. 10. Energy dependence of  $\Omega$  relative to pion. We compare our results with the Cleymans-Suhonen model [25]. Symbols are experimental data [26–29]. RHIC data are at midrapidity.

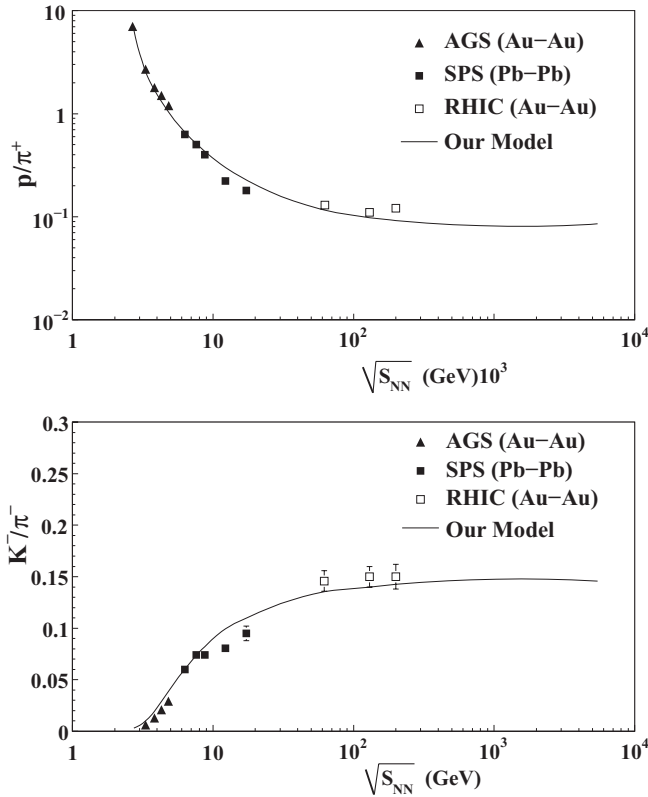


FIG. 11. Energy dependence of various hadrons relative to pion. Symbols are from experimental data [26–29] and the solid line represents our model calculation. RHIC data are at midrapidity.

$\sqrt{S_{NN}}$  and will become almost-equal at the LHC energy. The excellent agreements between our model results and the experimental data demonstrate the validity of our model for describing the data going from the lowest to the highest energy.

Usually excluded-volume models suffer from a severe deficiency caused by the violation of causality in a hot and dense HG, i.e., the sound velocity  $c_s$  is higher than the velocity of light  $c$  in the medium. In other words,  $c_s > 1$ , in units of  $c = 1$ , means that the medium transmits information at a speed faster than  $c$  [43]. It would be interesting to see if our model violates causality. In Fig. 13, we plot the variations of the total hadronic pressure  $P$  as a function of the energy density  $\epsilon$  of an HG at a fixed entropy per particle. We find that, for a fixed  $s/n$ , the pressure varies linearly with respect to the energy density. In Fig. 14, we show the variation of  $c_s$  ( $c_s^2 = \partial P/\partial \epsilon$  at a fixed  $s/n$ ) with respect to  $s/n$ . We find that  $c_s \leq 0.58$  always in our model of interacting particles having a hard-core size. We get  $c_s = 0.58$  (i.e.,  $1/\sqrt{3}$ ) for an ideal gas consisting of ultrarelativistic particles. This feature supports our viewpoint that our model not only is thermodynamically consistent but also does not involve any violation of causality.

In Fig. 15, we show the variations of nucleon density and pion density with respect to center-of-mass energy. We have compared our results with the IHG model and found that both results are in better agreement with the experimental data [44] as obtained by HBT interferometry. In fact, for the pion density, we find that the incorporation of hard-core size does not produce any noticeable change. However, for the

nucleon density, we note that our calculations yield results lying well below the HBT results at lower center-of-mass energies. Similarly, the experimental value for the nucleon density at RHIC energy lies well above our theoretical result. In general, the experimental data for enhanced nucleon density obtained in recent heavy-ion collider experiments have posed a problem which defies explanation. Hence, some other production mechanism is needed to explain the excess of baryon density observed in these experiments.

## V. FREEZE-OUT CRITERIA—REVISITED

In ultrarelativistic nucleus-nucleus collisions, a hot, dense matter is formed over an extended region for a very brief time and it is often called a “fireball.” The physical variables of the fireball are the volume  $V$ , energy density  $\epsilon$ , and baryon density  $n_B$ , which are in fact related to the  $T$  and  $\mu_B$  of the fireball. When cooling or expansion of the fireball starts, it goes through two types of freeze-out stages; when inelastic collisions between constituents of the fireball do not occur, we call this the chemical freeze-out stage. Later, when elastic collisions also cease to happen in the fireball, this stage is called the thermal freeze-out. The abundances of particles and their ratios provide important information regarding the chemical equilibrium occurring in the fireball just before thermal equilibrium.

After seeing the remarkable success of our model in explaining the multiplicities and the particle ratios of various particles produced in heavy-ion experiments from the lowest SIS energy up to the highest RHIC energies, we wish to extend the search for chemical freeze-out criteria for the fireball. Recently many papers have appeared [14,23,24,45–47] which predict the following empirical conditions to be valid on the entire freeze-out hypersurface of the fireball: (i) the energy per hadron is a fixed value at 1.08 GeV, (ii) the sum of the baryon and antibaryon densities  $n_B + n_{\bar{B}} = 0.12/\text{fm}^3$ , and (iii) the normalized entropy density  $s/T^3 \approx 7$ . Indeed, Cleymans *et al.* have found that these conditions separately give a satisfactory description of the chemical freeze-out coordinates of  $T$  and  $\mu_B$  in an IHG picture of statistical thermodynamics. Moreover, it was also proposed that these conditions are independent of the collision energy and the geometry of colliding nuclei, but these findings were not illustrated explicitly. Furthermore, Cleymans *et al.* [23] hinted that incorporation of the excluded-volume correction leads to wild as well as disastrous effects under these conditions. Our purpose in this section is to reinvestigate the validity of these freeze-out criteria in our excluded-volume model.

In Fig. 16, we show the variation of  $E/N$  with respect to the center-of-mass energy ( $\sqrt{S_{NN}}$ ) at the chemical freeze-out point of the fireball. The ratio  $E/N$  indeed shows a constant value of 1.0 in our calculation and it shows a remarkable energy independence. Similarly, the curve in the IHG model shows that the value for  $E/N$  is slightly larger than one reported in [23]. However, our results support that  $E/N$  is almost independent of the energy and, also, of the geometry of the nuclei. Most importantly, we note that the inclusion of the excluded-volume correction does not change

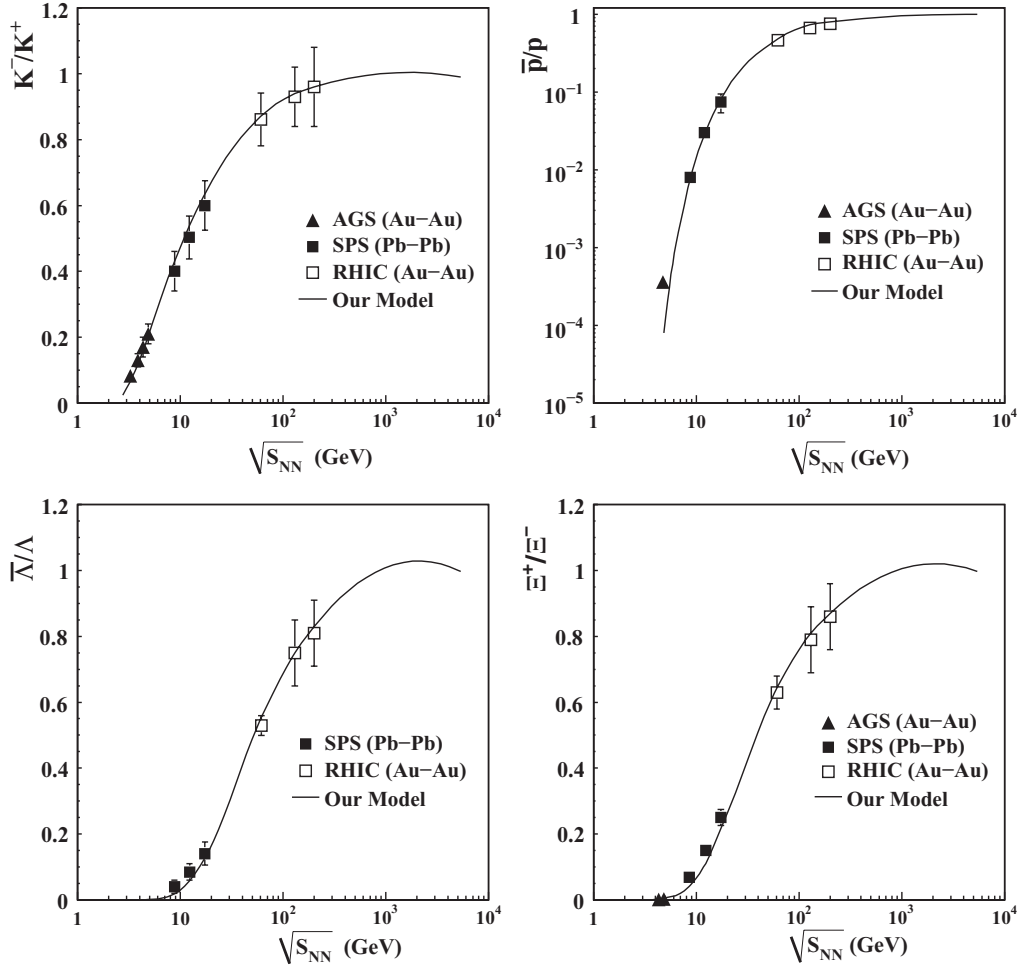


FIG. 12. Energy dependence of antihadron-to-hadron ratios. Symbols are from experimental data [26–29] and the solid line represents our model calculation. RHIC data are at midrapidity.

the result much, which is contrary to the claim of Cleymans *et al.* [23]. The condition  $E/N \approx 1.0$  GeV was successfully used in the literature to make predictions [48] of freeze-out parameters at SPS energies of 40 and 80 A GeV for Pb-Pb collisions long before the data were taken. Moreover, we also show in Fig. 16 the curves in the Cleymans-Suhonen model [25] and the RGSG excluded-volume model [14] and we note a small variation with  $\sqrt{S_{NN}}$ , particularly at lower energies.

In Fig. 17, we study a possible new freeze-out criterion which was not proposed earlier. We show that the quantity entropy per particle, i.e.,  $S/N$ , yields a remarkable energy independence in our model calculation. The quantity  $S/N \approx 7.0$  describes the chemical freeze-out criteria and is almost independent of the center-of-mass energy in our model calculation. However, the results below  $\sqrt{S_{NN}} = 6$  GeV do not give promising support for our criterion and show some energy dependence. This criterion thus indicates that the possible use of excluded-volume models and thermal descriptions at very low energies is not valid for HG. Similar results were obtained in the RGSG, Cleymans-Suhonen, and IHG models.

Should the normalized entropy density  $s/T^3$  remain fixed over the entire chemical freeze-out surface in heavy-ion colli-

sion experiments? This idea was initially used to extrapolate lattice gauge results from  $\mu_B = 0$  to finite values of  $\mu_B$  by keeping  $s/T^3$  fixed [47]. In Ref. [49] this quantity was also used to separate a baryon-dominant region from a meson-dominant one, in order to understand the rapid variations of certain particle ratios observed at lower SPS energies by the NA49 collaboration [30]. In Fig. 18, we show the energy dependence of the normalized entropy density  $s/T^3$ , which shows energy dependence at lower energies in almost all the models. In the IHG model, however, energy independence was observed to some extent and its value equals approximately 6.0. In the case of Cleymans-Suhonen and RGSG model calculations, this ratio follows the same trend as in our model calculation. This ratio varies wildly at lower energies in these excluded-volume models. Thus we cannot treat the criterion of fixed  $s/T^3$  as being valid on the freeze-out hypersurface of the fireball, as it is dependent on the energy of the collisions.

In heavy-ion collisions, the net baryon density, i.e., the difference between the density of baryons  $n_B$  and the density of antibaryons  $n_{\bar{B}}$ , shows wild variation with the center-of-mass energy as shown in Fig. 15. However, it was first noted by Braun-Munzinger *et al.* [45] that the sum of the baryon and antibaryon densities remains constant at chemical

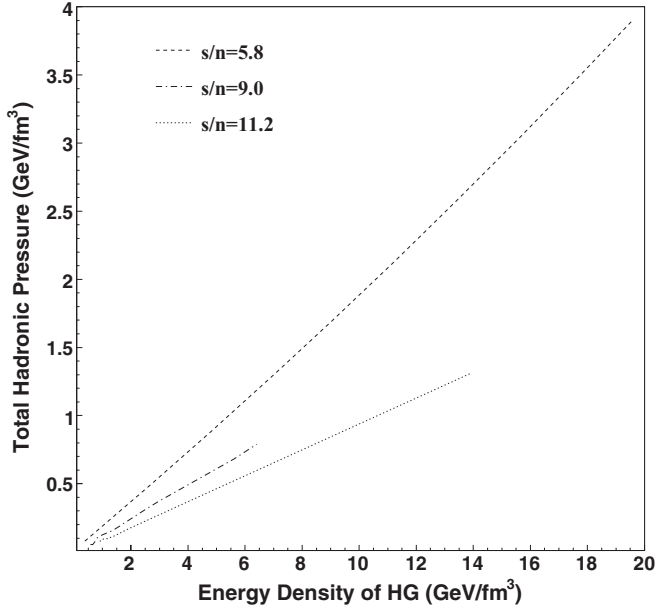


FIG. 13. Variations of the total hadronic pressure with respect to the energy density of an HG at a fixed entropy per particle  $s/n$ . Our calculations show a linear relationship and the slopes of the lines give the square of the velocity of sound  $c_s^2$ .

freeze-out. However, they used the excluded-volume model of RGSG and they used different eigenvolumes for baryons and mesons, respectively. In Fig. 19, we show the variation of  $n_B + n_{\bar{B}}$  with  $\sqrt{S_{NN}}$ . This quantity indeed involves a rapid variation with the energy in almost all the HG models. Our calculations thus reveal that some of the above criteria are not strictly valid on the freeze-out surface, as they do not show energy independence. However, as pointed out by certain authors, we can still treat them as freeze-out criteria

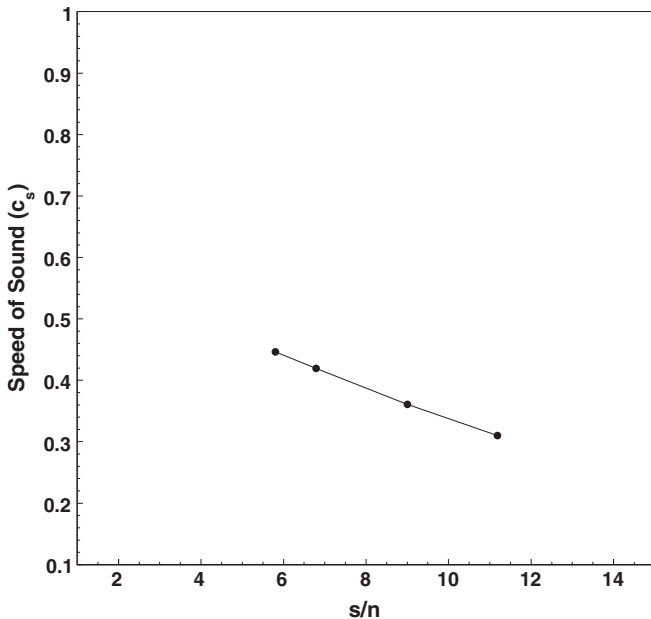


FIG. 14. Variation of the velocity of sound in a hot, dense HG medium with respect to the entropy per particle  $s/n$ .

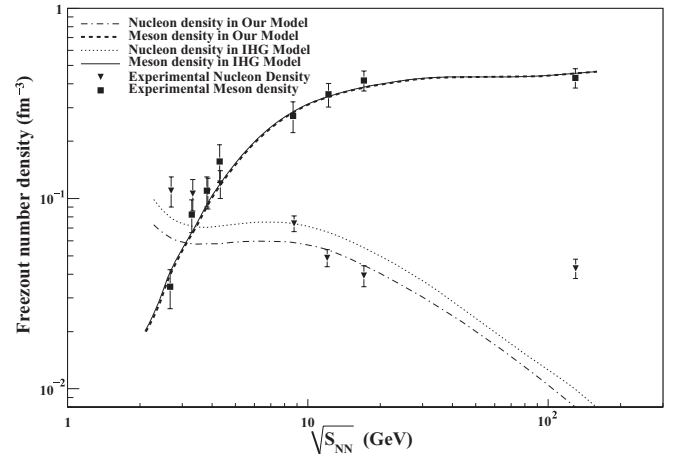


FIG. 15. Variation of nucleon density and pion density with respect to center-of-mass energy ( $\sqrt{S_{NN}}$ ). The solid line shows the meson density calculated in the IHG model and the dashed line shows our model calculation for meson density. Dotted and dash-dotted lines show the nucleon density calculated in the IHG model and our model, respectively. Filled symbols show HBT experimental data [44].

provided we give adjustable eigenvolumes for both baryons and mesons, respectively. Our finding lends support to the crucial assumption of achieving chemical equilibrium with an HG resulting in heavy-ion collisions from the lowest SIS up to the RHIC energy, and the EOS of the HG developed by us gives a proper description of the hot and dense fireball and its subsequent expansion. However, we still do not get any information regarding QGP formation from these criteria.

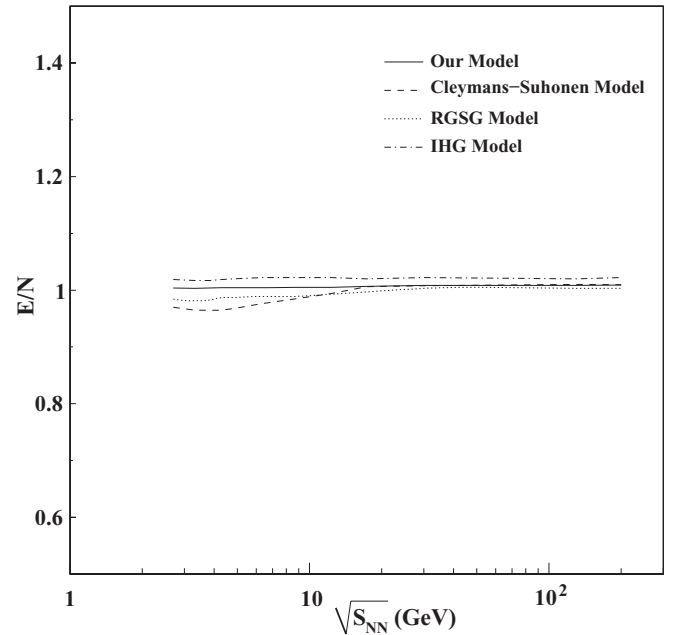


FIG. 16. Variation of  $E/N$  with  $\sqrt{S_{NN}}$ . The ideal HG model calculation is shown by the dash-dotted line; the Cleymans-Suhonen and Rischke *et al.* (RGSG) model calculations are shown by the dashed and dotted lines, respectively. The solid line shows the calculation using our model.

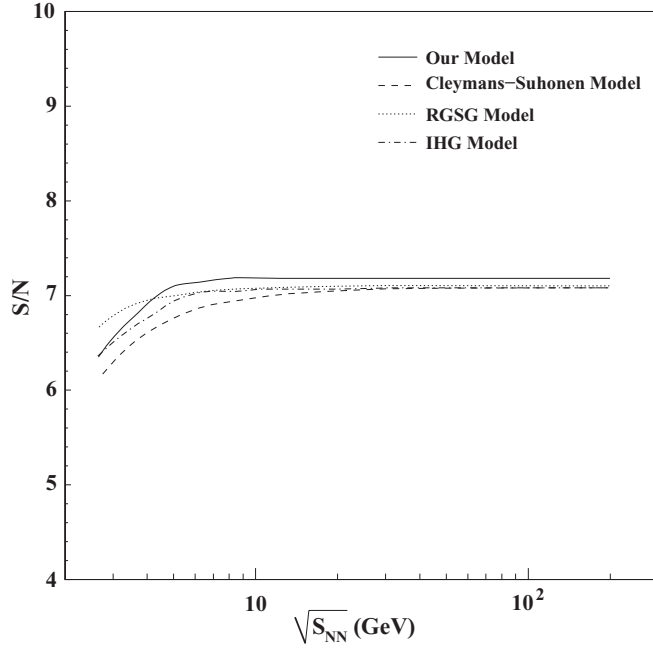


FIG. 17. Variation of  $S/N$  with  $\sqrt{S_{NN}}$ . The IHG model calculation is shown by the dash-dotted line; the Cleymans-Suhonen and Rischke *et al.* (RGSG) model calculations are shown by the dashed and dotted lines, respectively. The solid line shows the calculation using our model.

Once attained by a hot and dense HG, the chemical equilibrium removes any memory regarding QGP existing in the HG fireball. Furthermore, in a heavy-ion collision, a large amount

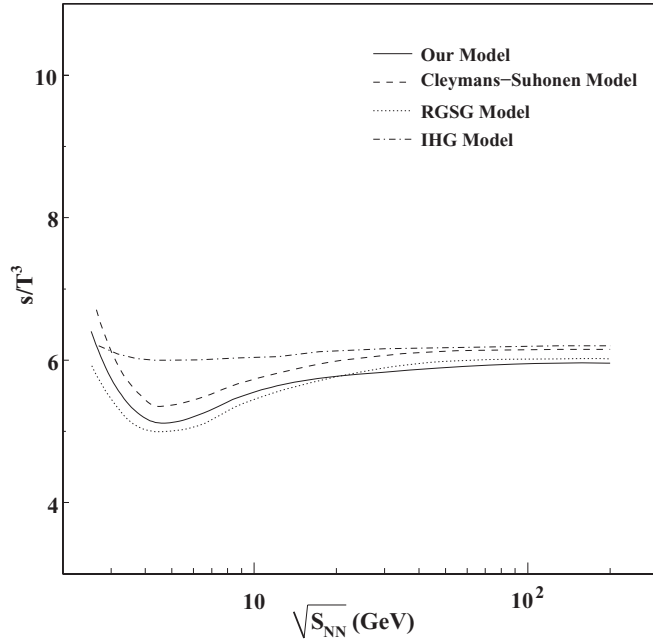


FIG. 18. Variation of  $s/T^3$  with  $\sqrt{S_{NN}}$ . The ideal HG model calculation is shown by the dash-dotted line; the Cleymans-Suhonen and Rischke *et al.* (RGSG) model calculations are shown by the dashed and dotted lines, respectively. The solid line shows the calculation using our model.

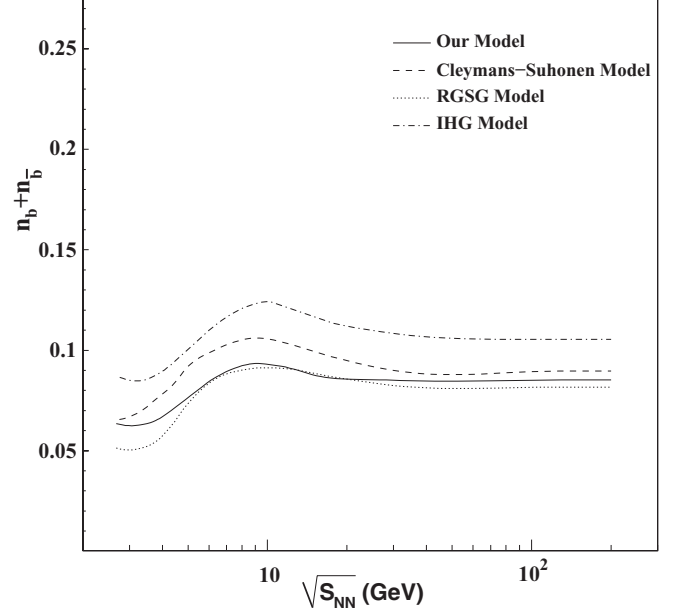


FIG. 19. Variation of  $n_b + n_{\bar{b}}$  with  $\sqrt{S_{NN}}$ . The ideal HG model calculation is shown by the dash-dotted line; Cleymans-Suhonen and Rischke *et al.* (RGSG) model calculations are shown by the dashed and dotted lines, respectively. Solid line shows the calculation using our model.

of kinetic energy becomes available and part of it is always lost during the collision due to dissipative processes. In the thermal description of the fireball, we ignore the effect of such processes and we assume that all available kinetic energy (or momentum) is globally thermalized at the freeze-out density. The experimental configuration of the collective flow in hot, dense matter reveals the unsatisfactory nature of the above assumption.

## VI. TRANSPORT PROPERTIES

Transport coefficients are of particular interest to quantify the properties of a strongly interacting relativistic fluid and its critical phenomena, i.e., phase transition, critical point, etc. [50–52]. The fluctuations cause the system to depart from equilibrium, and for a brief time a nonequibrated system is created. The response of the system to such fluctuations is essentially described by the transport coefficients, e.g., shear viscosity, bulk viscosity, and speed of sound. Recently the data on collective flow obtained from RHIC and LHC experiments indicate that the system created in these experiments behaves as a strongly interacting perfect fluid [53], whereas we expected that QGP created in these experiments would behave like a perfect gas. The perfect fluid created after the phase transition thus has a very low shear viscosity-to-entropy ratio value so that the dissipative effects are negligible and the collective flow should be large as obtained in heavy-ion-collision experiments [54,55]. There are several analytic calculations for  $\eta$  and  $\eta/s$  values of simple hadronic systems [56–62] along with some sophisticated microscopic transport model calculations [63–65] in the literature. Furthermore, some calculations predict that the minimum of the shear

viscosity-to-entropy density ratio is related to the QCD phase transition [66–70]. Similarly, the sound velocity is a very important property of the matter created in heavy-ion-collision experiments because the hydrodynamic evolution of this matter strongly depends on it. A minimum in the sound velocity has also been interpreted in terms of a phase transition [67,71–77], and further, the presence of a shallow minimum corresponds to a crossover transition [78]. Similarly, Liao and Koch have shown that the shear viscosity-to-entropy ratio cannot give a good measure of fluidity when one compares the relativistic vis-à-vis the nonrelativistic fluid, and they have defined a new fluidity variable for this purpose [79]. In view of the above, it is worthwhile to study in detail the transport properties of HG in order to fully comprehend the nature of the matter created in colliders as well as the phase transition phenomenon involved. In this section, our excluded-volume model for HG is used to calculate transport properties such as the shear viscosity-to-entropy ratio, the speed of sound, and also the fluidity measure as proposed by Liao and Koch [79].

Our calculation for the shear viscosity is completely based on the method of Gorenstein *et al.* [80], where the RGSG model was used for HG. According to molecular kinetic theory, we can write the dependence of the shear viscosity as [81]

$$\eta \propto n l \langle |\mathbf{p}| \rangle, \quad (14)$$

where  $n$  is the particle density,  $l$  is the mean free path, and hence the average thermal momentum of the baryons or antibaryons is

$$\langle |\mathbf{p}| \rangle = \frac{\int_0^\infty p^2 dp p \mathbf{A}}{\int_0^\infty p^2 dp \mathbf{A}}, \quad (15)$$

and  $\mathbf{A}$  is the Fermi-Dirac distribution function for baryons (antibaryons). For the mixture of particle species with different masses and with the same hard-core radius  $r$ , the shear viscosity can be calculated by the equation [80]

$$\eta = \frac{5}{64\sqrt{8} r^2} \sum_i \langle |\mathbf{p}_i| \rangle \times \frac{n_i}{n}, \quad (16)$$

where  $n_i$  is the number density of the  $i$ th species of baryons (antibaryons) and  $n$  is the total baryon density.

In Fig. 20, we show the variation of  $\eta/s$  with respect to temperature as obtained in our model for an HG having a baryonic hard-core size  $r = 0.5$  fm and compare the results with those of Gorenstein *et al.* [80]. We find that near the expected QCD phase transition temperature ( $T_c = 170$ – $180$  MeV),  $\eta/s$  shows a lower value in our HG model than in the other model. In fact,  $\eta/s$  in our model looks close to the lower bound ( $1/4\pi$ ) suggested by AdS/QCD theories [82]. Recently measurements in Pb-Pb collisions at the LHC support the value  $\eta/s \approx 1/4\pi$  compared with the viscous fluid hydrodynamic flow [83].

In Fig. 21, we show the variation of  $\eta/s$  with respect to  $\mu_B$  but at a very low temperature ( $\approx 10$  MeV). Here we find that the  $\eta/s$  is constant as  $\mu_B$  increases up to 700 MeV and then sharply decreases. This kind of valley structure at low temperatures and at a  $\mu_B$  of about 950 MeV was also obtained by Chen *et al.* and Itakura *et al.* [59,61]. They related this structure to the liquid-gas phase transition of the nuclear

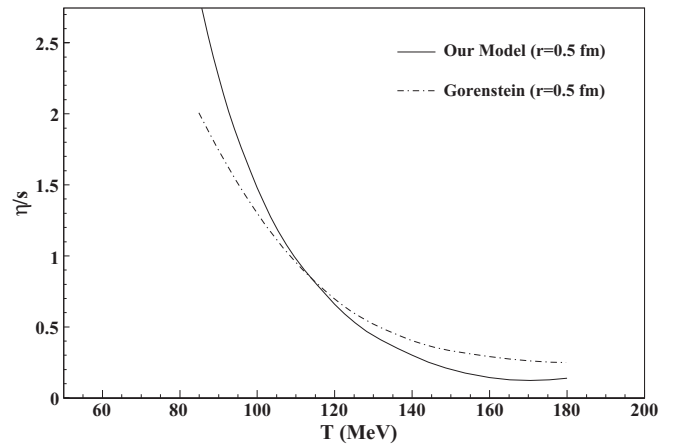


FIG. 20. Variation of  $\eta/s$  with temperature for  $\mu_B = 0$  in our model and a comparison with the results obtained by Gorenstein *et al.* [80].

matter. As we increase the temperature above 20 MeV, this valley-like structure disappears. They further suspect that the observation of a discontinuity in the bottom of the  $\eta/s$  valley may correspond to the location of the critical point. Our HG model yields a curve in complete agreement with these results.

In Fig. 22, we show the variation of  $\eta$  and  $\eta/s$  with respect to temperature at a fixed  $\mu_B$  ( $=300$  MeV) for an HG having a baryonic hard-core size  $r = 0.8$  fm and compare this result with the result obtained in Ref. [61]. Here we find that  $\eta$  increases with temperature in our HG model as well as in the simple phenomenological calculation in Ref. [61], but in low-temperature effective-field-theory calculations,  $\eta$  decreases with an increase in temperature [59,61]. However,  $\eta/s$  decreases with increasing temperature in all three calculations, and  $\eta/s$  in our model gives the lowest value at all temperatures in comparison with the other models.

In Fig. 23, we show a comparison between the  $\eta$  calculated in our HG model and the results obtained in the microscopic pion-gas model used in Ref [63]. Our model results show a

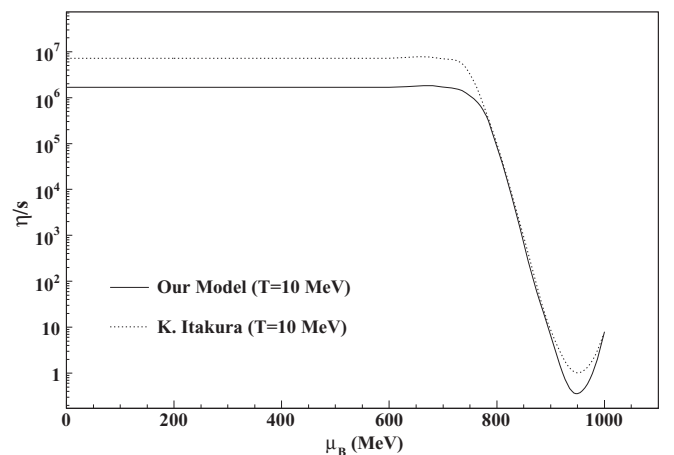


FIG. 21. Variation of  $\eta/s$  with respect to baryon chemical potential ( $\mu_B$ ) at a very low temperature, 10 MeV. The solid line represents our calculation and the dotted curve is that of Itakura *et al.* [61].

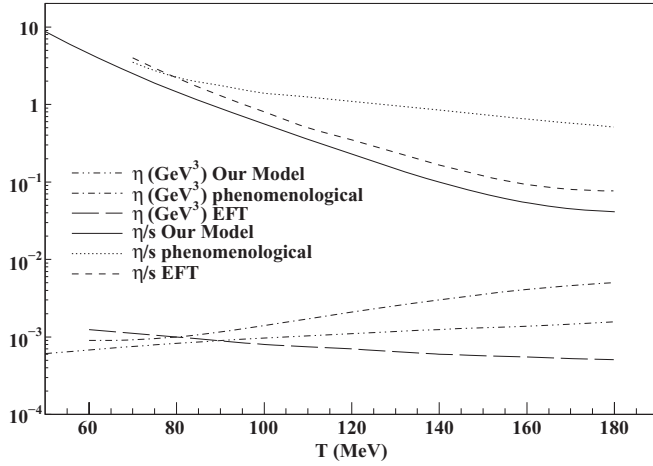


FIG. 22. Variation of  $\eta$  in units of  $(\text{GeV})^3$  and  $\eta/s$  with respect to temperature at  $\mu_B = 300$  MeV in our model and a comparison with the results obtained by Itakura *et al.* [61].

fair agreement with the microscopic model results for temperatures higher than 160 MeV, while at lower temperatures the microscopic calculation predicts lower values of  $\eta$  in comparison with our results. The most probable reason is that the calculations have been done only for pion gas in the microscopic model, while at low temperatures the inclusion of baryons in the HG is very important in order to extract the correct value for the shear viscosity.

The speed of sound is another important quantity because it is related to the speed of small perturbations produced in the medium in its local rest frame. Here we have used the recent formulation of Cleymans and Worku to calculate the speed

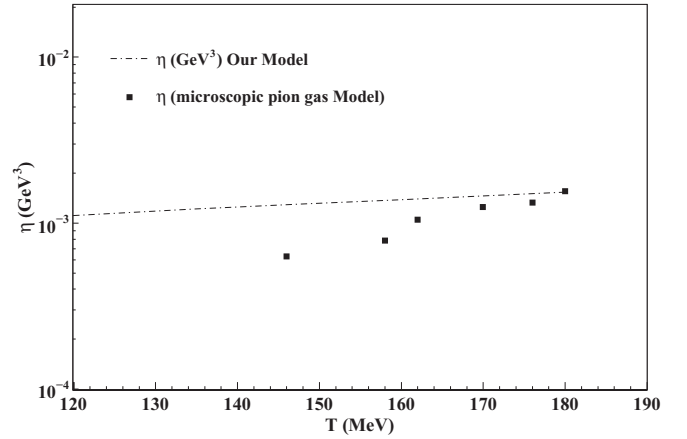


FIG. 23. Variation of  $\eta$  with respect to temperature at  $\mu_B = 300$  MeV in our model and a comparison with the results obtained by Muronga [63].

of sound at a constant  $s/n$  [72]. The speed of sound at zero chemical potential is easy to calculate where it is sufficient to keep the temperature constant [71,77]. However, the speed of sound ( $c_s$ ) at finite chemical potential can be obtained by using the extended expression [72]

$$c_s^2 = \frac{\left(\frac{\partial p}{\partial T}\right) + \left(\frac{\partial p}{\partial \mu_B}\right)\left(\frac{d\mu_B}{dT}\right) + \left(\frac{\partial p}{\partial \mu_s}\right)\left(\frac{d\mu_s}{dT}\right)}{\left(\frac{\partial \epsilon}{\partial T}\right) + \left(\frac{\partial \epsilon}{\partial \mu_B}\right)\left(\frac{d\mu_B}{dT}\right) + \left(\frac{\partial \epsilon}{\partial \mu_s}\right)\left(\frac{d\mu_s}{dT}\right)}, \quad (17)$$

where the derivative  $d\mu_B/dT$  and  $d\mu_s/dT$  can be evaluated by using two conditions: first, keeping  $s/n$  constant and, second, imposing overall strangeness neutrality. Thus one gets [72]

$$\frac{d\mu_B}{dT} = \frac{\left[n\left(\frac{\partial s}{\partial \mu_s}\right) - s\left(\frac{\partial n}{\partial \mu_s}\right)\right]\left[\frac{\partial L}{\partial T} - \frac{\partial R}{\partial T}\right] - \left[n\left(\frac{\partial s}{\partial T}\right) - s\left(\frac{\partial n}{\partial T}\right)\right]\left[\frac{\partial L}{\partial \mu_s} - \frac{\partial R}{\partial \mu_s}\right]}{\left[n\left(\frac{\partial s}{\partial \mu_B}\right) - s\left(\frac{\partial n}{\partial \mu_B}\right)\right]\left[\frac{\partial L}{\partial \mu_s} - \frac{\partial R}{\partial \mu_s}\right] - \left[n\left(\frac{\partial s}{\partial \mu_s}\right) - s\left(\frac{\partial n}{\partial \mu_s}\right)\right]\left[\frac{\partial L}{\partial \mu_B} - \frac{\partial R}{\partial \mu_B}\right]} \quad (18)$$

and

$$\frac{d\mu_s}{dT} = \frac{\left[n\left(\frac{\partial s}{\partial T}\right) - s\left(\frac{\partial n}{\partial T}\right)\right]\left[\frac{\partial L}{\partial \mu_B} - \frac{\partial R}{\partial \mu_B}\right] - \left[n\left(\frac{\partial s}{\partial \mu_B}\right) - s\left(\frac{\partial n}{\partial \mu_B}\right)\right]\left[\frac{\partial L}{\partial T} - \frac{\partial R}{\partial T}\right]}{\left[n\left(\frac{\partial s}{\partial \mu_B}\right) - s\left(\frac{\partial n}{\partial \mu_B}\right)\right]\left[\frac{\partial L}{\partial \mu_s} - \frac{\partial R}{\partial \mu_s}\right] - \left[n\left(\frac{\partial s}{\partial \mu_s}\right) - s\left(\frac{\partial n}{\partial \mu_s}\right)\right]\left[\frac{\partial L}{\partial \mu_B} - \frac{\partial R}{\partial \mu_B}\right]}, \quad (19)$$

where  $L = n_s^B + n_s^M$ , is the sum of the strangeness density for baryons and mesons. Similarly,  $R = n_s^{\bar{B}} + n_s^{\bar{M}}$ , the sum of the antistrangeness densities for baryons and mesons.

In Fig. 24, we show the variation of  $c_s^2$  with respect to  $\mu_B$  at two temperatures. We find that at  $T = 120$  MeV, there is a clear minimum at  $\mu_B \approx 500$  in the curve of the speed of sound, while in the case of  $T = 170$  MeV, we do not observe any such minimum and  $c_s^2$  continues to increase with increasing  $\mu_B$ . The minimum at  $\mu_B \approx 500$  for  $T = 120$  MeV indicates the position where a first-order phase transition from HG to QGP materializes.

In a recent paper [79], Liao and Koch suggested that  $\eta/s$  can serve as a good measure for the fluidity of a relativistic fluid

only because the ability of  $\eta/s$  to serve such a role is actually inherited from  $\eta/\omega$ , where the enthalpy of HG is  $\omega$ . We find that  $\omega$  becomes approximately equal to  $Ts$  only in the case of relativistic or ultrarelativistic matter. It is not always necessary for one to prefer  $\eta/s$  over  $\eta/\omega$  for a measure of the fluidity of the system. Thus if we want to compare various systems, i.e., relativistic and nonrelativistic, and extract some useful insights about the nature of the systems, then we have to define a fluidity measure exclusively in terms of the properties of the system itself. Liao and Koch defined a quantity  $F$  to measure the fluidity of a relativistic and/or nonrelativistic system as follows:

$$F = \frac{L_\eta}{L_n}, \quad (20)$$

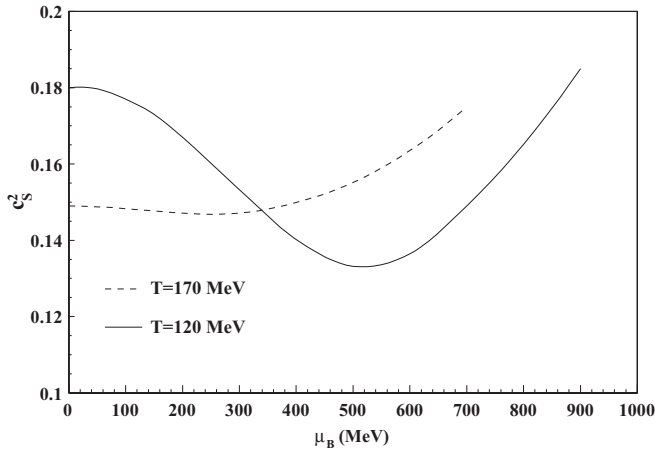


FIG. 24. Variation of the square of the speed of sound with respect to  $\mu_B$  at different temperatures.

where we can use

$$L_\eta = \frac{\eta}{\omega c_s}, \quad (21)$$

and  $L_n$  can be calculated by the relation [79]

$$L_n = \frac{1}{n^{1/3}} = \left(\frac{4}{s}\right)^{1/3}. \quad (22)$$

Actually  $L_\eta$  provides a measure for the minimal wavelength of a sound wave which propagates in a viscous fluid and  $L_n$  is basically related to the interparticle distance to provide an internal length scale for the medium. In Fig. 25, we show the variation of  $F = \frac{L_\eta}{L_n}$  with respect to temperature as obtained in our excluded-volume model using different hard-core sizes for baryons and compare the results with the curve obtained by Liao and Koch [79], in which they crudely assumed  $\eta/T_c^3 \approx T/T_c$ . We thus find that the features of our curves show a behavior similar to the results obtained by Liao and Koch using a completely different formalism.

Study of the transport properties of nonequilibrium systems which are not far from an equilibrium state has yielded valuable

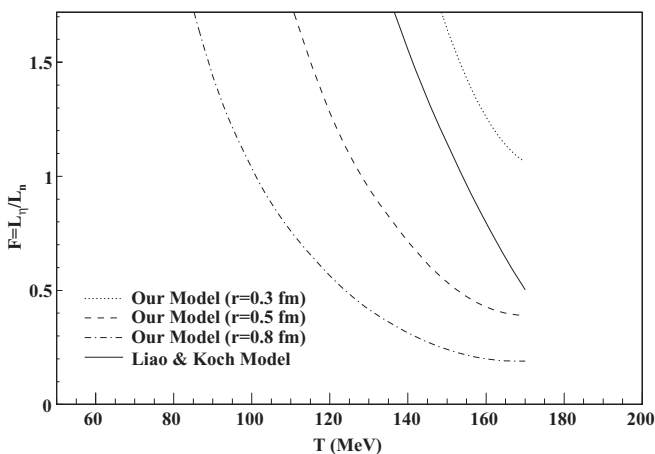


FIG. 25. Variation of fluidity ( $F$ ) with temperature for  $\mu_B = 0$  in our model and a comparison with the results obtained by Liao and Koch [79].

results in the recent past. The large values of the elliptic flow observed at the RHIC indicate that the matter in the fireball behaves as a nearly perfect liquid, with a low value of the  $\eta/s$  ratio. After evaluating  $\eta/s$  in strongly coupled theories using the AdS/CFT duality conjecture, the lower bound was reported as  $\eta/s = \frac{1}{4\pi}$ . We, surprisingly, note that a fireball with a hot, dense HG as described in our excluded-volume model gives a transport coefficient which agrees with those given by different approaches. The temperature and baryon chemical potential dependence of  $\eta/s$  are analyzed and compared with the results obtained with other models. We also focus our attention on  $c_s$  and the fluidity variable. Our results show trends and features similar to those reported by previous authors.

## VII. SUMMARY AND CONCLUSIONS

We have formulated a new thermodynamically consistent EOS for a hot and dense HG by incorporating a hard-core finite size of baryons and antibaryons only. We have treated mesons as pointlike particles. Alternatively, they possess a size but they can penetrate and overlap with each other. Our prescription is valid even at extreme values of  $T$  and  $\mu_B$ . Moreover, our model does not suffer from either of the two main inconsistencies, i.e., violation of causality and thermodynamic inconsistency. Our model involves a mathematical form which resembles the thermodynamically inconsistent Cleymans-Suhonen model but contains some extra correction terms which arise due to the condition of thermodynamic consistency. We have calculated the prediction of our model for various thermodynamic quantities, such as pressure, energy density, number density, and entropy density, and compared the predictions with those of other excluded-volume models. Similarly, we have also compared our results with those obtained from the microscopic simulation approach of Sasaki. We find that our results mostly show very close agreement with those of Sasaki, although the two approaches are completely different in nature. In addition, Sasaki's approach has a fundamental inconsistency and antibaryons and strange particles are not included in the model. The EOS thus formulated usually suffers from the crucial assumption regarding how many particles and resonances one should incorporate into it. We have taken all the known particles and resonances up to the mass of  $2 \text{ GeV}/c^2$ .

Our results for the particle ratios and their energy dependences fit the experimental data very well. We have deduced certain freeze-out criteria and attempted to test whether these criteria involve energy independence as well as independence of the structures of the nuclei involved in the collision. We find that two criteria, i.e.,  $E/N = 1.0 \text{ GeV}$  per produced particle and  $s/n = 7.0$ , demonstrate their validity. Moreover, the calculations of transport properties in our model match well with the results obtained using other widely different approaches.

In conclusion, the utility of our present model has been demonstrated in explaining various properties of a hot, dense HG, and thus our model provides a proper and realistic EOS for a hot, dense HG and it can suitably describe an HG at extreme values of temperatures and/or densities. Calculations regarding  $p_T$  as well as the rapidity spectra of different particles at the RHIC and LHC are still in progress and will be reported in a future paper.

## ACKNOWLEDGMENTS

S.K.T. and P.K.S. are grateful to the Council of Scientific and Industrial Research (CSIR), New Delhi, and University

Grants Commission (UGC) for providing a research grant. C.P.S. acknowledges the financial support through a project sanctioned by the Department of Science and Technology, Government of India, New Delhi.

- 
- [1] For introductory reviews on the subject, see C. P. Singh, *Phys. Rep.* **236**, 147 (1993); *Int. J. Mod. Phys. A* **7**, 7185 (1992).
- [2] M. J. Tannenbaum, *Rep. Prog. Phys.* **69**, 2005 (2006).
- [3] B. Muller, *Rep. Prog. Phys.* **58**, 611 (1995).
- [4] S. J. Lindenbaum and R. S. Longacre, *J. Phys. G* **26**, 937 (2000).
- [5] H. Satz, *Rep. Prog. Phys.* **63**, 1511 (2000).
- [6] P. Braun-Munzinger and J. Wambach, *Rev. Mod. Phys.* **81**, 1031 (2009).
- [7] P. Braun-Munzinger and J. Stachel, *Nature* **448**, 302 (2007).
- [8] M. Mishra and C. P. Singh, *Phys. Rev. C* **76**, 024908 (2007); **78**, 024910 (2008); *Phys. Lett. B* **651**, 119 (2007).
- [9] C. P. Singh, P. K. Srivastava, and S. K. Tiwari, *Phys. Rev. D* **80**, 114508 (2009); **83**, 039904(E) (2011).
- [10] P. K. Srivastava, S. K. Tiwari, and C. P. Singh, *Phys. Rev. D* **82**, 014023 (2010); arXiv:1101.1151v1 [hep-ph]; P. K. Srivastava, S. K. Tiwari, and C. P. Singh, *Nucl. Phys. A* **862-863**, 424 (2011).
- [11] N. Sasaki, *Prog. Theor. Phys.* **106**, 783 (2001).
- [12] A. Andronic, P. Braun-Munzinger, and J. Stachel, *Nucl. Phys. A* **772**, 167 (2006).
- [13] J. Cleymans and K. Redlich, *Phys. Rev. Lett.* **81**, 5284 (1998).
- [14] D. H. Rischke, M. I. Gorenstein, H. Stöcker, and W. Greiner, *Z. Phys. C* **51**, 485 (1991); R. Hagedorn, *ibid.* **17**, 265 (1983); G. D. Yen, M. I. Gorenstein, W. Greiner, and S. N. Yang, *Phys. Rev. C* **36**, 2210 (1997).
- [15] J. Cleymans and H. Satz, *Z. Phys. C* **57**, 135 (1993); J. Cleymans, H. Oeschler, and K. Redlich, *Phys. Lett. B* **485**, 27 (2000); P. Braun-Munzinger, D. Magestro, K. Redlich, and J. Stachel, *ibid.* **518**, 41 (2001).
- [16] P. Braun-Munzinger, K. Redlich, and J. Stachel, *Invited Review for Quark Gluon Plasma 3*, edited by R. C. Hwa and Xin-Nian Wang (World Scientific, Singapore, 2003); arXiv:nucl-th/0304013; P. Braun-Munzinger, J. Stachel, J. P. Wessels, and N. Xu, *Phys. Lett. B* **344**, 43 (1995); **365**, 1 (1996); J. Cleymans, D. Elliott, A. Keranen, and E. Suhonen, *Phys. Rev. C* **57**, 3319 (1998); J. Cleymans, H. Oeschler, and K. Redlich, *ibid.* **59**, 1663 (1999); R. Averbek, R. Holzmann, V. Metag, and R. S. Simon, *ibid.* **67**, 024903 (2003); J. Cleymans, H. Satz, E. Suhonen, and D. W. Von Oertzen, *Phys. Lett. B* **242**, 111 (1990); F. Becattini, M. Gazdzicki, and J. Sollfrank, *Eur. Phys. J. C* **5**, 143 (1998); G. Torrieri and J. Rafelski, *Phys. Lett. B* **509**, 239 (2001); G. Torrieri, S. Steinke, W. Broniowski, W. Florkowski, J. Letessier, and J. Rafelski, *Comput. Phys. Commun.* **167**, 229 (2005); S. Wheaton, J. Cleymans, and M. Hauer, *ibid.* **180**, 84 (2009); A. Kisiel, T. Taluc, W. Broniowski, and W. Florkowski, *ibid.* **174**, 669 (2006).
- [17] F. Becattini, J. Cleymans, A. Keranen, E. Suhonen, and K. Redlich, *Phys. Rev. C* **64**, 024901 (2001).
- [18] C. Spieles, H. Stöcker, and C. Greiner, *Eur. Phys. J. C* **2**, 351 (1998).
- [19] B. Schenke and C. Greiner, *J. Phys. G* **30**, 597 (2004).
- [20] W. Florkowski, W. Broniowski, and M. Michalec, *Acta Phys. Pol. B* **33**, 761 (2002); W. Broniowski and W. Florkowski, *Phys. Rev. C* **65**, 064905 (2002).
- [21] C. P. Singh, B. K. Patra, and K. K. Singh, *Phys. Lett. B* **387**, 680 (1996); S. Uddin and C. P. Singh, *Z. Phys. C* **63**, 147 (1994).
- [22] A. Andronic, P. Braun-Munzinger, J. Stachel, and H. Stöcker, *Phys. Lett. B* **697**, 203 (2011).
- [23] J. Cleymans, H. Oeschler, K. Redlich, and S. Wheaton, *Phys. Rev. C* **73**, 034905 (2006); J. Cleymans *et al.*, *Phys. Lett. B* **660**, 172 (2008).
- [24] J. Cleymans and K. Redlich, *Phys. Rev. C* **60**, 054908 (1999).
- [25] J. Cleymans and E. Suhonen, *Z. Phys. C* **37**, 51 (1987).
- [26] C. Alt *et al.*, *Phys. Rev. C* **77**, 024903 (2008).
- [27] C. Alt *et al.*, *Phys. Rev. C* **78**, 034918 (2008); C. Blume (for the NA49 Collaboration), *J. Phys. G* **31**, S685 (2005).
- [28] M. M. Aggarwal *et al.*, *Phys. Rev. C* **83**, 024901 (2011).
- [29] A. Andronic *et al.*, *Nucl. Phys. A* **837**, 65 (2010).
- [30] M. Gazdzicki (NA 49 Collaboration), *J. Phys. G* **30**, S701 (2004).
- [31] S. V. Afanasiev *et al.* (NA 49 Collaboration), *Phys. Rev. C* **66**, 054902 (2002).
- [32] T. Anticic *et al.*, *Phys. Rev. Lett.* **93**, 022302 (2004).
- [33] L. Ahle *et al.* (E 802 Collaboration), *Phys. Rev. C* **57**, 466 (1998); (E 802 Collaboration), **60**, 044904, 064901 (1999); (E 802 Collaboration), **60**, 064901 (1999); (E 866/E 917 Collaboration), *Phys. Lett. B* **490**, 53 (2000).
- [34] S. Albergo *et al.*, *Phys. Rev. Lett.* **88**, 062301 (2002); S. Ahmad *et al.*, *Phys. Lett. B* **381**, 35 (1996); J. Klay *et al.* (E 895 Collaboration), *Phys. Rev. C* **68**, 054905 (2003).
- [35] R. Stock, *J. Phys. G* **30**, S633 (2004).
- [36] J. Noronha-Hostler, H. Ahmad, J. Noronha, and C. Greiner, *Phys. Rev. C* **82**, 024913 (2010).
- [37] P. Braun-Munzinger, J. Cleymans, H. Oeschler, and K. Redlich, *Nucl. Phys. A* **697**, 902 (2002).
- [38] J. K. Nayak, S. Banik, and J. Alam, *Phys. Rev. C* **82**, 024914 (2010).
- [39] M. Gazdzicki, *J. Phys. G* **30**, S161 (2004).
- [40] E. Bratkovskaya *et al.*, *Phys. Rev. C* **69**, 054907 (2004).
- [41] V. Koch, A. Majumder, and J. Randrup, *Phys. Rev. C* **72**, 064903 (2005).
- [42] D. Molnar and S. A. Voloshin, *Phys. Rev. Lett.* **91**, 092301 (2003); D. Molnar, *J. Phys. G* **30**, S1239 (2004); L. W. Chen and C. M. Ko, *Phys. Rev. C* **73**, 044903 (2006); V. Greco, C. M. Ko, and P. Levai, *Phys. Rev. Lett.* **90**, 202302 (2003).
- [43] N. Prasad, K. K. Singh, and C. P. Singh, *Phys. Rev. C* **62**, 037903 (2000).
- [44] D. Admova *et al.* (CERES Collaboration), *Phys. Rev. Lett.* **90**, 022301 (2003).
- [45] P. Braun-Munzinger and J. Stachel, *J. Phys. G* **28**, 1971 (2002); P. Braun-Munzinger, I. Heppke, and J. Stachel, *Phys. Lett. B* **465**, 15 (1999).
- [46] V. Magas and H. Satz, *Eur. Phys. J. C* **32**, 115 (2003).
- [47] A. Tawfik, *J. Phys. G* **31**, S1105 (2005).
- [48] K. Redlich and A. Tounsi, *Eur. Phys. J. C* **24**, 589 (2002).
- [49] J. Cleymans, H. Oeschler, K. Redlich, and S. Wheaton, *Phys. Lett. B* **615**, 50 (2005).

- [50] J. Kapusta, *Phys. Rev. C* **24**, 2545 (1981); M. Prakash, R. Venugopalan, and G. Welke, *Phys. Rep.* **227**, 321 (1993).
- [51] A. M. Polyakov, *J. Exp. Theor. Phys.* **57**, 2144 (1969).
- [52] F. Karsch, D. Kharzeev, and K. Tuchin, *Phys. Lett. B* **663**, 217 (2008).
- [53] U. W. Heing and P. F. Kolb, *Nucl. Phys. A* **702**, 269 (2002); A. Adare *et al.* (PHENIX Collaboration), *Phys. Rev. Lett.* **98**, 172301 (2007); T. Hirano and M. Gyulassy, *Nucl. Phys. A* **769**, 71 (2006).
- [54] M. Gyulassy and L. McLerran, *Nucl. Phys. A* **750**, 30 (2005); E. V. Shuryak, *ibid.* **750**, 64 (2005).
- [55] P. Romatschke and U. Romatschke, *Phys. Rev. Lett.* **99**, 172301 (2007).
- [56] S. Gavin, *Nucl. Phys. A* **435**, 826 (1985).
- [57] A. Dobado and S. N. Santalla, *Phys. Rev. D* **65**, 096011 (2002).
- [58] M. Prakash, M. Prakash, R. Venugopalan, and G. Welke, *Phys. Rep.* **227**, 321 (1993).
- [59] J.-W. Chen, Y.-H. Li, Y.-F. Liu, and E. Nakano, *Phys. Rev. D* **76**, 114011 (2007).
- [60] J.-W. Chen and E. Nakano, *Phys. Lett. B* **647**, 371 (2007).
- [61] K. Itakura, O. Morimatsu, and H. Otomo, *Phys. Rev. D* **77**, 014014 (2008).
- [62] A. S. Khvorostukhin, V. D. Toneev, and D. N. Voskresensky, *Nucl. Phys. A* **845**, 106 (2010).
- [63] A. Muronga, *Phys. Rev. C* **69**, 044901 (2004).
- [64] S. Muroya and N. Sasaki, *Prog. Theor. Phys.* **113**, 457 (2005).
- [65] N. Demir and S. A. Bass, *Phys. Rev. Lett.* **102**, 172302 (2009).
- [66] L. P. Csernai, J. I. Kapusta, and L. D. McLerran, *Phys. Rev. Lett.* **97**, 152303 (2006).
- [67] J. Noronha-Hostler, J. Noronha, and C. Greiner, *Phys. Rev. Lett.* **103**, 172302 (2009).
- [68] R. A. Lacey *et al.*, *Phys. Rev. Lett.* **98**, 092301 (2007).
- [69] A. Dobado, F. J. Llanes-Estrada, and J. M. Torres-Rincon, *Phys. Rev. D* **79**, 014002 (2009); **80**, 114015 (2009).
- [70] S. Pal, *Phys. Lett. B* **684**, 211 (2010).
- [71] P. Castorina, J. Cleymans, D. E. Miller, and H. Satz, *Eur. Phys. J. C* **66**, 207 (2010).
- [72] J. Cleymans and D. Worku, *Mod. Phys. Lett. A* **26**, 1197 (2011).
- [73] R. V. Gavai and A. Gocksch, *Phys. Rev. D* **33**, 614 (1986).
- [74] K. Redlich and H. Satz, *Phys. Rev. D* **33**, 3747 (1986).
- [75] F. Karsch, PoS **CPOD07**, 026 (2007).
- [76] P. Braun-Munzinger and J. Stachel, *Nucl. Phys. A* **606**, 320 (1996).
- [77] D. Prorok and L. Turko, [arXiv:hep-ph/0101220](https://arxiv.org/abs/hep-ph/0101220).
- [78] M. Chojnacki and W. Florkowski, *Acta Phys. Pol. B* **38**, 3249 (2007).
- [79] J. Liao and V. Koch, *Phys. Rev. C* **81**, 014902 (2010).
- [80] M. I. Gorenstein, M. Hauer, and O. N. Moroz, *Phys. Rev. C* **77**, 024911 (2008).
- [81] E. M. Lifschitz and L. P. Pitaevski, *Physical Kinetics*, 2nd ed. (Pergamon Press, Oxford, 1981), chap. 1, p. 3.
- [82] G. Policastro, D. T. Son, and A. O. Starinets, *Phys. Rev. Lett.* **87**, 081601 (2001); J. M. Maldacena, *Adv. Theor. Math. Phys.* **2**, 231 (1998); P. K. Kovtun, D. T. Son, and A. O. Starinets, *Phys. Rev. Lett.* **94**, 111601 (2005).
- [83] Z. Qiu, C. Shen, and U. W. Heinz, [arXiv:1110.3033](https://arxiv.org/abs/1110.3033) [nucl-th].